EUROPEAN ORGANIZATION FOR NUCLEAR RESEARCH

CERN/ISRC 73-28
1 October 1973

PROPOSAL TO STUDY ELECTROMAGNETIC PROPERTIES OF PROTONS IN THE TIME-LIKE REGION AND TO SEARCH FOR THE NEUTRAL BOSON Z^0 *)

G. Diambrini-Palazzi, U.J. Becker, P J. Biggs,
A. Cook, G. Everhart, P. Goldhagen, R. Little,
K. Strauch and S.C C. Ting

Genoa-Harvard-MIT Collaboration

---

*) Together with the Pisa-Stony Brook Group, we are designing a possible hadron detector to be used in conjunction with the present experiment Preliminary investigation revals that a 4π hadron detector measuring virtual photon-hadron correlations, using most of the existing Pisa-Stony Brook equipment, can be readily arranged together with the muon detector.

In this proposal we present a set-up to study

$$p + p \rightarrow \gamma_v + X \quad , \qquad \gamma_v \rightarrow \mu^+ + \mu^- \qquad (1)$$

by measuring the mass and angular distribution of the heavy photon $\gamma_v \rightarrow \mu^+\mu^-$ in the mass region $1 < m < 15$ GeV. Information on the structure of X will also be obtained.

A second aim is to search for

$$p + p \rightarrow Z^0 + Y \quad , \qquad Z^0 \rightarrow \mu^-\mu^+ \qquad (2)$$

up to Z^0 mass of 37 GeV, where Z^0 is the neutral heavy boson responsible for the existence of leptonic and hadronic neutral currents[1-9].

This proposal outdates our previous proposal[10] to perform the experiment at the SFMD. Without the limitation of SFMD, we have designed a detector which is simple, covers a larger solid angle (8.4 sr), detects μ pairs with small opening angles down to $2\theta \approx 30^\circ$, has a more uniform and well-known magnetic field, involves smaller π-μ decay distances, and permits the sampling of hadron showers and the measurement of multiple scattering, etc. These features, which will enable us to perform a more systematic study, permit many more system checks and control our experimental conditions.

Figure 1 shows the set-up of the muon detector: muons are detected and analysed by iron toroids with uniform circular field of 17 kG and no field on the ISR beams. Spark chambers sandwiched between the toroids identify hadrons and large-angle Coulomb scattered muon pairs from hadron decays. The decay distance is reduced to a minimum by placing magnetic iron shielding next to the bicone.

The unique features of this detector are as follows:

1) It covers an angular region $15^\circ < \theta < 110^\circ$ which enables us to detect very forward $\mu^-\mu^+$ pairs. (So far no lepton pairs, bosons, etc., have

The advantage of studying reactions (3) and (4) comes from the fact that one has a clear initial state of a time-like photon ($C = -1$, $J = 1$), $P = -1$) decaying into hadrons. It is clear that reactions (3) and (4) are closely related to reactions (1) and (2), respectively.

The production of heavy photons in pp collisions is closely related to deep inelastic electron scattering by many models in the literature In these current models the production of heavy photons is due to parton-antiparton annihilation; the properties of the partons are inferred from

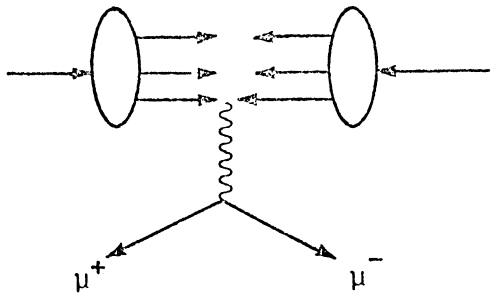

$Q(Q_0, Q_1, Q_2, Q_3)$

$Q^2 = m_\gamma^2$; $Q_3 = p_{||}$

the results of the deep inelastic electron scattering experiments According to this picture the study of the production of heavy photons thus picks out the parton-antiparton collision channel among the many involved in the collisions of one parton system with another

These general remarks indicate the great interest of studying the production of heavy photons at the ISR; we will now discuss the predictions of some specific models to serve as a guide to determine kinematic regions of particular interest and to obtain estimates of the event rates

The models yield a functional dependence of the form:

$$\frac{d^2\sigma}{dm_\gamma^2 dQ_3} = \frac{4\pi\alpha^2}{3m_\gamma^4 Q_0} \sum_{a,\bar{a}} \frac{F_{2a}(x_1)F_{2\bar{a}}(x_2)}{\lambda_a^2} \quad .$$

λ_a is a constant determined by the previous μ pair and e pair experiments. The function $F_{2a}(x_1)$ is determined by the SLAC deep inelastic scattering data[11]. Many models assume that the two functions $F_{2a}(x_1)$ and $F_{2\bar{a}}(x_2)$ are equal (Kuti-Weisskopf, Drell-Yan, Landshoff-Polkinghorn) [12]; this assumption produces good agreement with the BNL data on $P + U \to \mu^+ + \mu^- + X$ [13]. On the other hand, the difference in the νN and $\bar{\nu}N$ [14] scattering data can be explained by a difference in the distribution functions $F_{2a}(x)$ and $F_{2\bar{a}}(\bar{x})$ [E. Paschos, Llewellyn-Smith [15]]. This assumption of asymmetric distribution of partons and antipartons will

strongly favour forward (and backward) moving γ_v. Thus the $p_{\parallel}$ dependence of the production cross-section of heavy photons is related to the difference between the functions $F_{2a}(x_1)$ and $F_{2\bar{a}}(\bar{x}_2)$. For example, the model of Paschos which takes the $\bar{\nu}N$ data into account would imply that all the $m_\gamma > 1$ GeV pairs have $p_{\parallel} > 8$ GeV and maximum opening angle of $\theta_\mu = 54°$ only, and will not be seen by a 90° detector. At $m \approx 5$ GeV the two distributions yield the same $p_{\parallel}$ dependence.

Because of the current uncertainties in the models, it is important to have the detector cover forward regions and 90° regions together. The small opening angle of the detector will enable us to collect $4 < m_\gamma < 6$ GeV events with high statistics allowing us to also study the $p_\perp^2$ dependence of γ_v. Comparison of $p_\perp$ dependence of γ_v production with the corresponding dependence in π, K, p production will yield important information on the nature of the interaction of time-like photons with protons.

Rate calculations based on these models will be presented later.

1.2 Study X distribution

We know of no theoretical work on the structure of X in reaction (1). However, when the photon is in the space-like region ($q^2<0$) in the reaction $e + p \to e + p + X$, there are many experiments[16] on X. These experiments have yielded the following (at W = mass of X ≈ 3 GeV, forward direction, $0 < |q|^2 < 1$).

i) The multiplicity decreases with increasing $|q^2|$;

ii) no change in strange particle ratio;

iii) vector mesons disappear with increasing $|q^2|$;

iv) π^+/π^- ratio increases with $|q^2|$;

v) the proton yield is independent of $|q^2|$.

It would be interesting to study X in reaction (1), when the photon is in the time-like region.

1.3 The search for Z^0

Recent development in unified gauge theories[1-9] of weak and electromagnetic interactions have been fruitful in focusing attention on the existence of neutral heavy bosons Z^0. Different models require different

mass of Z^0. The Bjorken-Llewellyn-Smith and Lee-Prentki-Zumino model[5-7], require both Z^0 and heavy leptons. There is no theoretical lower bound on the mass of Z^0. Primack and Quinn[17] have analysed the g-2 experiment for electrons and muons and have found that the present experimental accuracy limits the mass of the Z^0 to $m_{Z^0} > 10$ GeV.

Z^0 should couple directly to $\mu^+\mu^-$. The width of Z^0 is $\Gamma = \alpha m_{Z^0}$; the integrated production cross-section of $Z^0 \to \mu^+\mu^-$ of reaction (2) is enhanced over $\gamma_v \to \mu^-\mu^+$ production of reaction (1) by the usual (mass/width) factor of $(\pi/\alpha)q^2/(m_{Z^0})^2 \approx 400$. This factor enables us to search for $\mu^-\mu^+$ enhancement up to mass of $m_{Z^0} \approx 37$ GeV, where the $\gamma_v \to \mu^-\mu^+$ yields have already vanished.

2. EXPERIMENTAL SET-UP

Figure 1 shows the set-up of muon detector. It has the following main features:

1) Following the designs of W. Panofsky (Appendix A), the eight iron toroids A, B, C, D, E, F, G, H are made to have a uniform magnetic field of 17 kG in circular direction around the ISR with no field on the ISR beams. The toroids are made in pieces for easy assembly. The toroids measure μ momenta and reject hadrons. The magnetic field inside the toroids can be monitored by placing probes inside the small air gaps between the iron pieces. Toroids of similar size have been used in three NAL experiments with success.

Toroids A, B, C, D, E are circular in shape. The inner radii are from 30 cm to 65 cm, where the outer radius is 2.0 m, and Fig. 2 shows the end view of section E. The thickness of A is 20 cm; B, C, D, E are 40 cm, toroid H (Fig. 3) is also circular in shape so that there is no stray field on the bicone. The inner radius of H is 38 cm, permitting four conventional Charpak chambers to be easily installed.

There are two possible geometries for toroids G and F. The circular shape as shown in Fig. 4 requires eight rectangular chambers and a $\sim$ 10% loss of ϕ acceptance. The toroids will have a very uniform field. The square shapes as shown in Fig. 5 require only four rectangular chambers to have the complete ϕ coverage. The loss of the ϕ angle will be $\sim$ 5%.

But the detailed magnetic field on the corners will have to be studied more completely.

The removal of block (I) will increase the $\pi,K \to \mu$ decay length by factor of 2 (factor of 4 for pairs), and this will provide a useful check on decay and hadronic shower backgrounds.

3) The locations of the triggering counters are shown in Fig. 1. The S counters form a cylindrical ring, with radius 18 cm, surrounding the bicone. This hodoscope S has 36 elements, each 3.14 cm wide, 80 cm long, 0.5 cm thick (Fig. 6a). Hodoscopes P and R each have 36 elements, with dimensions $45 \times 180 \times 2$ cm^3. The P-counters form a square box, surrounding toroids F, A, and B. The R-counters surround toroids B, C, D, and E. The arrangement of P is shown also in Fig. 5. Hodoscope Q has also 36 elements, each shown in Fig. 6b. The 36 Q-counters form a circular fan surrounding the front part of toroid E.

Figure 7 shows a perspective view of the counters. The triggering design is based on the following considerations:

i) The toroids provide a circular field; the bending of μ's is in the polar direction and does not affect the azimuthal angle.

ii) Worst multiple (1σ) scattering lateral displacement (at $\theta = 37°$, 4 GeV) is 7 cm.

iii) Because γ_v and Z^0 production from reactions (1) and (2) are strongly peaked at $p_\perp < 1$ GeV, the decayed $\mu^+\mu^-$ tend to have large azimuthal angle between them. (For $p_\perp = 0$, $p_{\mu^+} = p_{\mu^-}$, then the azimuthal angle between $\mu^+\mu^-$ is 180°).

iv) Rejection of cosmic-ray and beam-gas backgrounds in the trigger.

Each of the hodoscope banks has 36 elements. Each element subtends an azimuthal angle of 10°. The simplest trigger (T) would be:

$$\text{define } \mu^+ \text{ trigger } T_i^+ = S_i(P_{i-1} + P_i + P_{i+1}) \text{ or } S_i(R_{i-1} + R_i + R_{i+1}) \text{ or } S_i(Q_{i-1} + Q_i + Q_{i+1});$$

similarly for T_j^-;

and $T = (T_i^+)(T_j^-)$ with $|i - j| > 9$, so $\mu^+\mu^-$ are at least 90° apart in azimuthal angle, and one can tighten the trigger during the experiment

by requiring the $\mu^+\mu^-$ azimuthal angle to be large. Beam-gas backgrounds are rejected as trigger T requires two very high energy hadron showers hitting Q-counters from upstream and penetrating 2 m of iron to fire the two S-counters located at least 90° apart.

4) The chambers: The functions of the chambers C_1-C_{10} are fivefold:

i) To measure the invariant mass of $\mu^-\mu^+$ pairs by measuring the momentum and angle of each particle.

ii) To reject large-angle single scattering of muons from $\pi, K \to \mu$ decays.

iii) To reject hadron showers by monitoring the angle and momenta of the track when it passes through the toroids. The secondary hadrons that deviate from the original path by an amount much larger than bending and multiple scattering thus can be easily rejected

iv) To reject single cosmic rays passing through the bicone which will leave a straight track in C_4. By requiring the two muons to have a collinearity angle $< 173°$, a rejection factor of $\sim 10^4$ is obtained for cosmic rays.

v) To track the muons through toroids in order to obtain better resolution.

The large chambers C_1 are 4 m × 4 m drift chambers with 10 cm wire spacing and a 5 cm ground plate spacing. A total of nine planes in a space of 50 cm will provide rejection for left-right ambiguity and multiparticle confusions, and will provide an angular resolution $\theta \approx 1$ mrad. These chambers will be copies of the current chambers used for the NAL neutrino experiment.

The chambers C_{10} are 2 m × 4 m drift chambers with 10 cm wire spacing and with signal wires parallel (and perpendicular) to the B field of the toroids for maximum momentum resolution; nine planes will provide an angular resolution of $\theta \approx 1$ mrad matching the resolution of the chambers C_1.

Chambers C_4 and C_5 are Charpak chambers, with an angular resolution of $\approx 1°$, which measure the initial track directions. They consist of six planes rotated 60° with respect to each other so as to obtain maximum rejection of multitrack ambiguities.

Chambers C_2, C_3, C_6, C_7, C_8, C_9 are drift chambers, constructed in the same way as C_{10} chambers but with closer sense wire spacing (5 cm) to

provide closer ground plate spacing. There are three planes in each chamber to provide a unique determination of the location of tracks.

The system will be monitored with a large existing PDP 11/45 for which most of the software is already written.

3. RATE CALCULATIONS

To understand the rate dependence of reactions (1) and (2) on various models and their energy dependence, we calculate the yield on 200 hours of running at 2×10^{30} cm^{-2} sec^{-1} luminosity with the model of:

A) Jaffe and Primack[18], which assumes that the partons and antipartons have the same distribution;

B) Paschos[13], which takes into account the $\sigma_{\bar{\nu}N}/\sigma_{\nu N} \approx 1/3$ observation by assuming different distribution functions for partons and antipartons, and this favours forward μ pair production.

Both (A) and (B) formulae, in the form of $d^2\sigma/dm^2dp_{\parallel}$, have been checked by Paschos and Llewellyn-Smith[13]. We use a Monte Carlo program to calculate the yield of $\mu^+\mu^-$ as a function of mass, taking into account loss of energy and Coulomb scattering. The result for ISR beams of 26 + 26 GeV is shown in Fig. 8a. From Fig. 8a we make the following observations:

i) the two models give very similar results for low mass photons;

ii) most of events are centred at $m_\gamma = 5 \pm 1$ GeV where we can study the $p_\perp$ dependence of γ_v.

We next perform calculations based on the model of Jaffe and Primack on the five most commonly used ISR energies of 11+11, 15+15, 22+22, 26+26, and 31+31 GeV. The results are shown in Figs. 8b,c. We note that for $m_\gamma < 8$ GeV (Fig. 8b) the yield is rather insensitive to the ISR energies. It increases by a factor of 3 from 11+11 GeV to 31+31 GeV This means we will be able to collect $\gamma_v \to \mu^-\mu^+$ data whenever the ISR is used for experiment. For $m_\gamma > 20$ GeV the $\gamma_v \to \mu^+\mu^-$ yield vanishes. Since the $Z^0 \to \mu^+\mu^-$ yield is enhanced over the $\gamma_v \to \mu^+\mu^-$ by $(\pi/\alpha)q^2/m_{Z^0}{}^2$ one can still search for $Z^0 \to \mu^+\mu^-$. Figure 8c shows the Z^0 yield as a function of ISR energies. As seen, to search for Z^0 we need to run the ISR above 15+15 GeV.

4. MACHINE TIME REQUIREMENT

From Figs. 8a,b and the remarks above we plan to request 1000 hours of data-taking time arranged roughly in the following way:

> 1000 hours above 15+15 GeV, detailed division between 26+26 GeV and 22+22 GeV not important, though 26+26 GeV is preferred.

Figures 9 and 10 show the $\gamma_v \to \mu^-\mu^+$ and $Z^0 \to \mu^-\mu^+$ event rate, respectively, with the above running schedule (we have used the model of Jaffe and Primack with 500 hours at 26+26 GeV, 400 hours at 22+22 GeV, both at 2×10^{30} cm^{-2} sec^{-1}; and 31+31 GeV, 100 hours, 5×10^{29} cm^{-2} sec^{-1}. This schedule follows the 1972 pattern).

Assuming an $e^{-6p_\perp}$ (same as $p + p \to \pi^+ + X$ at ISR) dependence for $p + p \to \gamma_v + X$, we obtain the $p_\perp$ distribution shown in Fig. 11. As seen if γ_v behave like hadrons, we can study the $p_\perp$ dependence up to $p_\perp \approx 1$ GeV.

5. BACKGROUND CONSIDERATIONS

There are three main backgrounds to be taken into account:

1) cosmic-ray background
2) $\pi, K \to \mu$ decay
3) hadron showers.

We discuss each one separately.

5.1 Cosmic-ray background

The measured vertical muon cosmic-ray spectrum[19] at sea level is shown in Fig. 12. From these data we find that the rate of random muon pairs going through the intersection region is negligible. The rate for cosmic-ray muons with energy > 4 GeV passing through the intersection region and the detector is about 2000 per hour From the experience of the single muon experiment[20] we know that more than 99% of them will be rejected on line by TOF techniques between the P-, R-, Q-, and S-counters. (Off line one gains a factor of 10 or more in rejection.) Furthermore, single-muon cosmic-ray background can be eliminated by rejecting particles produced exactly at 180° with respect to each other in the laboratory.

A Monte Carlo program was used to simulate cosmic rays going through the proportional chambers C_4. We found that the chance of confusing a pair, with opening angle less than 173°, with a single track is less than 10^{-4}. If we discard all events with opening angle greater than 173°, the single cosmic-ray background/1000 hours is 1000 × 2000 × 1/100 (on-line timing) × 1/10 (off-line timing) × 10^{-4} = 0.2/1000 hours, which is 100 times smaller than the yield at $m_{Z^0} \approx 30$ GeV. Additional rejection can be obtained by noting that a single cosmic ray passing through the iron surrounding the bicone loses ∿ 2 GeV of energy: thus the event has a $p_\perp \approx 2$ GeV. By making a $p_\perp$ cut of 1 GeV we reject this event. Note that although a heavy particle like Z^0 produced almost at rest prefers to decay into a muon pair back to back in the c.m. system, when it is transformed into the laboratory system the preferred value in the opening is around 170°, depending on the crossing angle of the ISR beams. The loss of events due to the 7° cut is therefore negligible.

5.2 Decay background

This background is reduced to a minimum by noting that in the set-up (Fig. 1) we have:

i) The shortest possible decay path.

ii) We measure the position of the track every 20-40 cm of iron. This enables us to reject large-angle scattering.

To calculate the $\pi, K \to \mu$ contribution, we used the measured π, K spectrum from ISR [21] and use the correlation factors measured on $\pi^0\pi^0$ [22] from the CCR group and for forward angles from the Winter group[23]. For very large angles where the $p_\perp > 8$ GeV, there is no experimental data and we have assumed $d\sigma/dp_\perp = d\sigma/dp_\perp\ (p_\perp = 8\ \text{GeV}) = \text{constant}$.

The decay contribution was calculated with the Monte Carlo method using the program of Øverås[24], which treats the problem of Coulomb scattering in large confined bodies, taking into account not only the Gaussian term but also all other no-Gaussian tails $[(a/\Psi^3) + (b/\Psi^5) \ldots]$. Energy loss is also taken into account and we reject low-energy muons by range. The resultant $\mu^-\mu^+$ yields are shown in Fig 9. As seen, the decay background is ∿ 1% of the expected yield for m > 3 GeV. Most of

the high mass background comes from two muons from $\pi, K \to \mu$ decays; each muon experiences a large-angle scattering in one of the toroids and together they appear as a high mass $\mu^-\mu^+$ pair. The information on large-angle scattering from the position of tracks between toroids will enable us to reduce this background still further. By performing angular cuts accepting events in the $20° < \theta < 110°$ region instead of the $15° < \theta < 110°$ will also reduce the background considerably.

5.3 Hadron showers

The problem of high-energy hadrons interacting in material to produce more hadrons has been studied experimentally by many groups[25]; for example, Geibel et al. at CERN measured the hadron distribution on a 3.2 m stack of steel. Ranft has developed an empirical program to fit this data[26].

Our ability to follow the track through the toroids will reduce the hadron penetration to a negligible level.

To estimate this background we take the following steps:

i) generate $p\pi$, $\pi\pi$, K^-K^+ pairs in the same way as before;

ii) use Øverås' program to follow a muon track through the chambers;

iii) use Ranft's empirical formula to calculate the chance that a p, π, K shower will reach the outside triggering counters and the chance that a secondary hadron will stay within 2 standard deviations of the muon tracks.

The results of this calculation are shown in Fig. 9. It can be seen that compared to the expected rate, this background is down to the 1/1000 level.

6. RESOLUTION IN MOMENTUM AND MASS

The resolution is determined by the amount of multiple scattering, since both bending, $\theta_B = [0.03\ B\ell\ (kG\ m)]/p(GeV)$, and multiple scattering, $\theta_M = [0.015/p(GeV)]\sqrt{\ell/\ell_0}$, are inversely proportional to momentum p The resolution, to zeroth order, is given by $\Delta p/p = \theta_M/\theta_B \propto 1/(B\sqrt{\ell})$ and improves slowly with ℓ independently of p

Measuring the coordinates between the toroids will somewhat improve $\Delta p/p$.

Using the chamber information on angle and coordinates, taking into account the multiple scattering, energy loss, and bending, a fitting program was written to study the resolution in momentum and mass. Figure 13a shows the $\Delta p/p$ results at $\theta_\mu = 37°$, where we have the largest bending and multiple scattering angles: we obtain a $\Delta p/p = 16\%$ FWHM. Figure 13b shows the result at 90° where we have the smallest bending and multiple scattering angles: we obtain a $\Delta p/p = 20\%$ FWHM. From this we obtain values $\Delta M/M = (11\text{-}14)\%$ FWHM.

7. OPTIONS

1) For simplicity we have arranged to have all the triggering counters outside the toroids -- this leads to a $p_{min} = 2$ GeV. We can rearrange to have the triggering counters sandwiched between the toroids to trigger on $p_{min} = 1.5$ GeV. This will increase the total yields by factor of 3. This can be done if all the background calculations are realistic and if the yield of reactions (1) and (2) should be much smaller than the theories predict.

2) The inner iron block (I), Fig. 1, can be rearranged, and the hodoscope S and C_4 chamber enlarged, permitting us to study correlations of γ_v with X in the forward region down to 15°.

8. REQUIREMENT ON THE ISR

1) We will be able to start setting up this experiment in spring 1975.

2) The beam pipes in the toroids can be thick, and bake-out equipment can be permanently left on the beam pipes.

Acknowledgements

Professor W.K.H. Panofsky participated in many interesting physics discussions and designed the magnets for this experiment, but because of his short stay at CERN, he is not able to participate in its future development. We are grateful to have had the experience of working with him and for the many interesting ideas he has contributed to this proposal.

We thank also Drs. F. Bonaudi, J. Burger and S.L. Wu for many interesting discussions.

APPENDIX (by W K.H. Panofsky)

A. GENERAL MAGNET DESIGN CONSIDERATIONS

The magnet is to give full coverage in azimuth in order to provide a large solid angle well in excess of other lepton pair experiments and cover a range in production angle θ given by $15^\circ < \theta < 110^\circ$. As discussed in the proposal, this latter value provides a large range in muon-pair mass and is desirable in view of the absence of theoretical models in whose prediction as to angular distribution one might have confidence.

There are substantial advantes in a) full azimuthal symmetry, and b) in a uniform magnetic field. A large part of the gain is in terms of track fitting computer time; other advantages are: saving in steel weight and simplicity of fabrication. Primary disadvantage is a difficult geometry for locating the required track chambers near the 90° region.

Iron core toroids were chosen as magnetic analysers. They serve the dual role of muon absorbers and momentum analysers, and require a minimum of excitation windings and are economical in power. The ratio of magnetic deflection $\delta\theta$ to projected r.m.s. scattering angle $\langle\theta\rangle$ in magnetized iron, is roughly given by

$$\frac{\delta\theta}{\langle\theta\rangle} = 0.24\ B_T \ell^{\frac{1}{2}} ,$$

where B_T is the magnetic induction in teslas, and ℓ is in cm. An iron path length of 2 m (ionization energy loss = 2.3 GeV) in a field of 1.7 T gives $\delta\theta/\langle\theta\rangle = 5.8$; the results of such calculations emphasize the need for a uniformly high flux density, since if part of the iron is excited to a low field it will contribute a disproportionate amount to scattering. The attainable momentum resolution with a 2 m path is thus roughly 17% divided by the square root of the number of wire planes crossed by the muons which is generally 3. Thus, a 10% (1σ) momentum resolution appears attainable.

The designs in this proposal are based on simple analytic calculation. Due to the simplicity of design these should be fully reliable;

however, it is anticipated to produce detailed flux plots using the POISSON program produced at LBL and available at CERN.

A further requirement is that of a magnetic field in the interaction region sufficiently low to meet ISR criteria. Toroidal rings operating at induction values of 1.7 T will have values of H near 60 Oe; depending on the distribution of windings, the field in the central hole will be well below this value; moreover, a very thin shield pipe operating at such low fields can fully remove any perturbing field.

Total weight of the five forward toroids is 170 tons. Total power requirement is estimated near 120 kW.

B. TOROID DESIGN FOR THE SMALL-ANGLE REGION (Fig. 2)

Geometrical constraints indicate an outer diameter (o.d.) of 400 cm and on inner diameter (i.d.) of 130 cm. Moreover, the ISR interaction region geometry indicates a slightly elongated hole since small-angle muons and likely to be distributed symmetrically about the direction of the "forward" beam. Without disturbing the basic design principle, this problem was solved by the addition of a 20 cm "straight" section to the circular toroid. To maintain a uniform flux density, the use of a variable air gap appears indicated. If the toroids are to operate at a uniform field of 1.7 T, two gaps varying radially from 1.61 cm at the i.d. to 0.11 cm at the o.d. will make the total reluctance independent of radius. Two coils, each of about 3.25×10^4 Ampere-turns, placed around the gap will excite the toroid to 1.7 T. At 500 A/cm^2 the coil area might be about 60 cm^2 for each of the two coils and the power consumption would be about 30 kW/coil for a toroid width of 1 m and a 50% winding efficiency. Other coil configurations are, of course, possible. With a two-coil configuration and without a magnetic shield, the field inside the toroid's i.d. will exhibit three null lines with the field in between these lines possibly rising to 15 gauss.

C. THE MAGNETIC TOROIDS FOR THE ANGULAR REGION NEAR 90°

In the small-angle region the principal component of magnetic deflection is perpendicular to the beam axis; hence a single toroid can span the entire radial interval, with detection chambers placed between toroids in planes perpendicular to the axis. In the region near 90° the principal component of magnetic deflection is parallel to the axis; thus it appears desirable to break the toroids into three annular rings in order to permit insertion of chambers into the iron path. This requirement, together with mechanical needs, poses special problems. We indicate two solutions, both of which are fully feasible. These solutions are:

1) three circular magnetic rings;

2) one circular magnetic annulus surrounded by two near-rectangular magnetic frames.

Solution 1

The inner ring is common to both solutions: it is a toroid of 76 cm i.d. and 160 cm o.d. This leaves ample space (Fig. 3) for the placement of proportional chambers in a rectangular frame about the beam. The same considerations as discussed above indicate two air gaps tapering from 0.57 cm to 0.10 cm; two coils, each of 1.2×10^4 Ampère-turns, will drive the toroid to 1.7 tesla.

The two additional toroids are placed to permit space for chambers in the intervening region. The problem is the choice of the appropriate chambers. Naturally, chambers of circular symmetry are preferred; however, the resolution requirement is high (about 3 mm along the axis); circular chambers constructed to date have their wires run parallel or near-parallel (SLAC-SPEAR) to the axis; this results in inadequate resolution for this purpose. If the drift chambers using a helical delay-line as a collector, now under development by Charpak and collaboration, prove successful in providing adequate resolution in the sizes (near 1 m length) needed here, this may be the correct solution; both Charpak and ourselves are optimistic that this can be demonstrated Pending development of delay-line drift chambers, a layout (Fig. 4) locating eight chambers in the annular air space appears fully feasible and will only

lose a few per cent in azimuthal coverage due to the width of the wire chamber frames. The three iron rings have the following specifications:

	Inner diameter (cm)	Outer diameter (cm)	Gap widths (2 gap)		Ampère turns/coil (two coils)
			inner (cm)	outer (cm)	
H	76	160	0.57	0.10	1.2×10^4
G	200	290	0.60	0.10	2.3×10^4
F	330	400	0.49	0.10	3.1×10^4

Total power consumption of all six coils combined will be near 100 kW, depending on detailed design. Total weight will be about 80 tons.

Solution 2

In case the circular delay-line drift chambers prove difficult to develop and in case the large number of plane chambers (eight per annular space) are undesirable, magnets G and H could be of square shape (Fig. 5); the inner magnet F should remain circular to avoid stray fields at the ISR beam. A square design poses some magnetic design problems if the iron is to be effectively utilized If a simple square frame is energized, the field along the corner diagonals will be weaker by a factor of roughly $\sqrt{2}$ than the average, and the inside corner will saturate; we estimate that for an average 1.7 T flux density the fields will exceed 2.0 T for a distance away from the inside corner of about 20% of the width of the frame.

A rectangular frame should therefore be modified by chopping the corner to provide approximately uniform width; gussets placed inside the corners could reduce the saturation. However, since the inside toroid (H) will remain circular, the increased stray field implied by saturation will not reach the ISR. If it is decided, in the interest of chamber simplicity, to adopt the rectangular solution, the design will be carefully mapped with POISSON.

D. MAGNETIC MEASUREMENTS

The flux density in the toroids should be measured to the 3% level of accuracy. It appears that, with this design, this can be achieved by the installation of Hall probes in the two air gaps of the toroids, thus permitting continuous monitoring. Extrapolation of these Hall probe readings to the magnetic induction in the toroids should be fully reliable at the desired level of accuracy, provided extensive mapping of the stray field and calculation with POISSON of the toroids verifies that the external fields are indeed as low as predicted.

REFERENCES

1) A. Salam, in Elementary Particle Theory, edited by N. Svartholm (Almquist and Forlag, Stockholm, 1968)..

2) S. Weinberg, Phys. Rev Letters 19, 1264 (1967); 27, 1688 (1971); Phys Rev D5, 1412 (1972); 5, 1962 (1972)

3) G. 't Hooft, Nuclear Phys. B35, 167 (1971).

4) H. Georgi and S.L Glashow, Phys. Rev. Letters 28, 1494 (1972).

5) B.W. Lee, Phys. Rev. D6, 1188 (1972).

6) J. Prentki and B Zumino, Nuclear Phys. B47, 99 (1972).

7) For references to some of the other papers on this subject which had appeared in early 1972, see: B W. Lee, NAL Report No. THY-34, 1972 (invited paper presented at the San Francisco meeting of the APS, 1972); C.H. Llewellyn-Smith, in Proc. 4th Int Conf. on High-Energy Collisions, Oxford, 1972 (Oxford Univ. Press, to be published).

8) T.D. Lee, Phys. Rev. Letters 26, 801 (1971)

9) J. Schwinger, Phys. Rev. 7, 908 (1972).

10) P.J. Biggs et al., CERN ISRC/73/9; ISRC/73/9 Add. 1; ISRC/73/9 Add. 2.

11) H. Kendall, Raporteur's talk, Int. Conf. on Electromagnetic Interactions, Cornell, 1971.

12) J.D. Drell and T.M. Yan, Phys. Rev Letters 25, 316 (1970).
J. Kuti and V F Weisskopf, Phys Rev. D4, 3418 (1971).
P.V. Landshoff and J C. Polkinghorne, Phys. Letters 40 B, 463 (1972)

13) H.H. Christenson et al., Phys. Rev. Letters 25, 1523 (1970).

14) CERN-Gargamelle-Collaboration (presented by V. Brisson, 16th Int. Conf. on High-Energy Physics, Chicago-Batavia, 1972 (NAL, Batavia, 1973), Vol. 3, p. 195.

15) E. Paschos and C. Llewellyn-Smith, private communication.

16) G. Wolf, DFSY 72/61, 1972, and D. Luke, private communication

17) J. Primack and H. Quinn, Phys. Rev. Letters D6, 3171 (1972).

18) R. Jaffe and J Primack, Nuclear Phys. B, to be published.

19) P.J. Hayman and A.W. Wolfendale, Proc. Phys. Soc. 80, 710 (1962).

20) We thank Dr. P. Sharp for this information.

21) British-Scandinavian ISR Collaboration, Production of high transverse momentum particles in p-p collisions in the central region at the CERN ISR, CERN preprint March 1973
M.G. Albrow et al., Longitudinal momentum distributions for positive particles produced at small angles in proton-proton collisions at a centre-of-mass energy of 44.6 GeV, CERN preprint, August 1972.

22) F.W. Busser et al., Int. Conf. on New Results from Experiments on High-Energy Particle Collisions, Vanderbilt University, Nashville 26-28 March, 1973.

23) H. Dibon et al., Correlations between photons and charged particles measured at the CERN ISR, CERN preprint, August 1973.

24) CERN Internal Report SC/146 (1957).

25) B.D. Hyams et al., Phys. Letters 24 B, 634 (1967).
A. Wehmann et al., Phys. Rev. Letters 17, 1113 (1966).
For more work on hadron attenuation, see: A. Citron et al., Nuclear Instrum. Methods 32, 45 (1965) and M. Tannenbaum, Nevis-132 (1965).

26) J. Geibel et al., Nuclear Instrum. Methods 32, 48 (1965).
J. Ranft, Nuclear Instrum Methods 48, 261 (1967)

Figure captions

Fig. 1 : Side view of the $\mu^-\mu^+$ detector.

Fig. 2 : End view of toroid E.

Fig. 3 : End view of toroid H, together with chambers C_4.

Fig. 4 : End view of circular toroids F, G, H together with chambers.

Fig. 5 : End view of square toroids F, G, H together with chambers.

Fig. 6a : Hodoscopes S_i.

Fig. 6b : Hodoscopes Q_i.

Fig. 7 : Perspective view of the muon detector.

Fig. 8 : Monte Carlo result of event rates from $p + p \rightarrow \mu^+\mu^- + X$:
a) comparison of the Paschos and Jaffe models at 26+26 GeV, 2×10^{30} cm^{-2} sec^{-1}, 200 hours;
b) yield of $\gamma_v \rightarrow \mu^-\mu^+$ Jaffe model as function of energy, at 2×10^{30} cm^{-2} sec^{-1}, 200 hours each energy;
c) yield of Z^0 in Jaffe model as function of energy, at 2×10^{30} cm^{-2} sec^{-1}, 200 hours each energy.

Fig. 9 : Expected event rates as a function of $m_{\mu\mu}$.

Fig. 10 : Event rates from Z^0 as a function of m_{Z^0}.

Fig. 11 : $p_\perp$ dependence of events in Fig. 9.

Fig. 12 : Vertical cosmic-ray spectrum at sea level.

Fig. 13a : Monte Carlo result of FWHM of the best momentum resolution for muons.

Fig. 13b : Monte Carlo result of FWHM of the worst momentum resolution for muons.

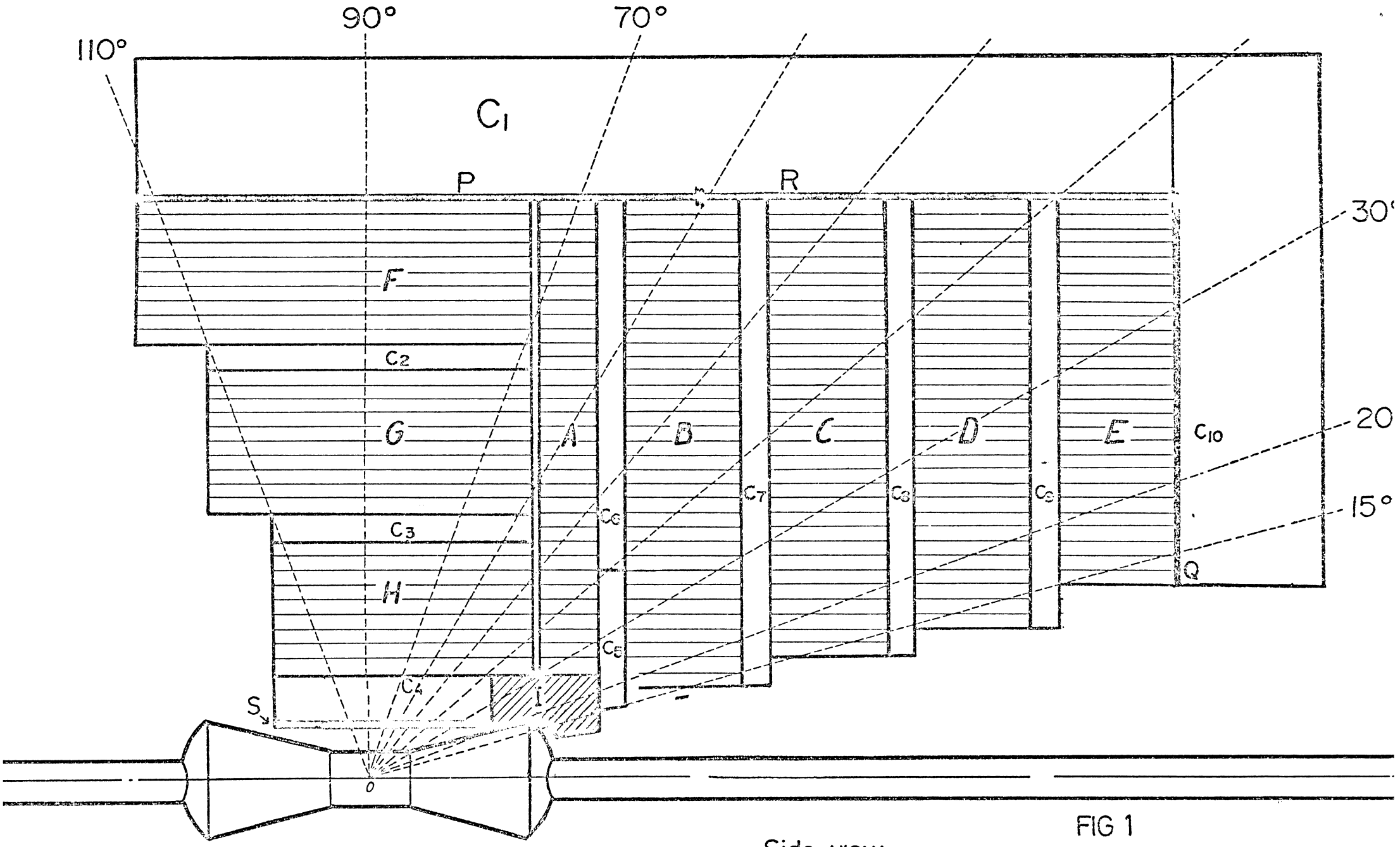

FIG 1

Side view

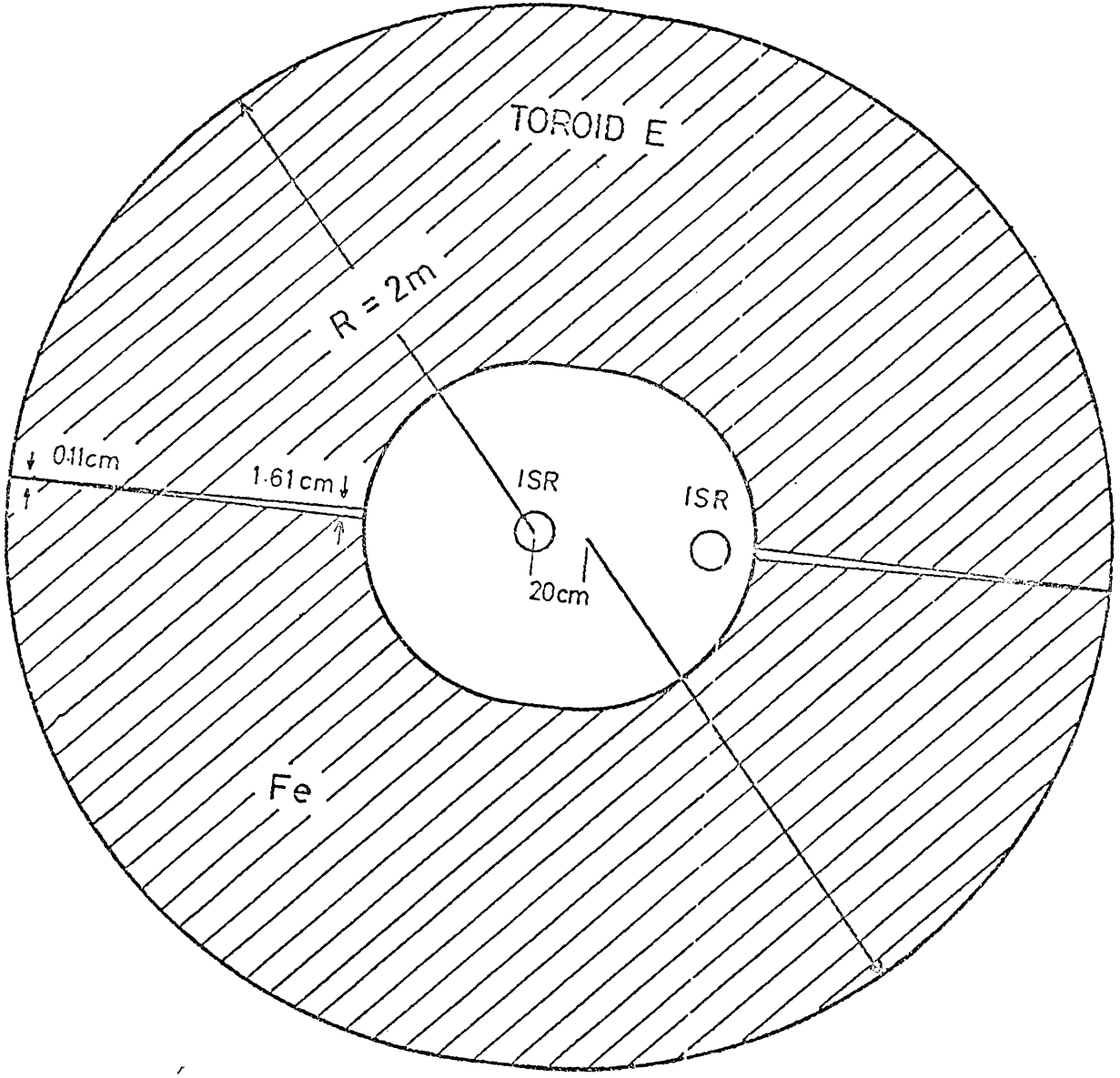

Fig. 2

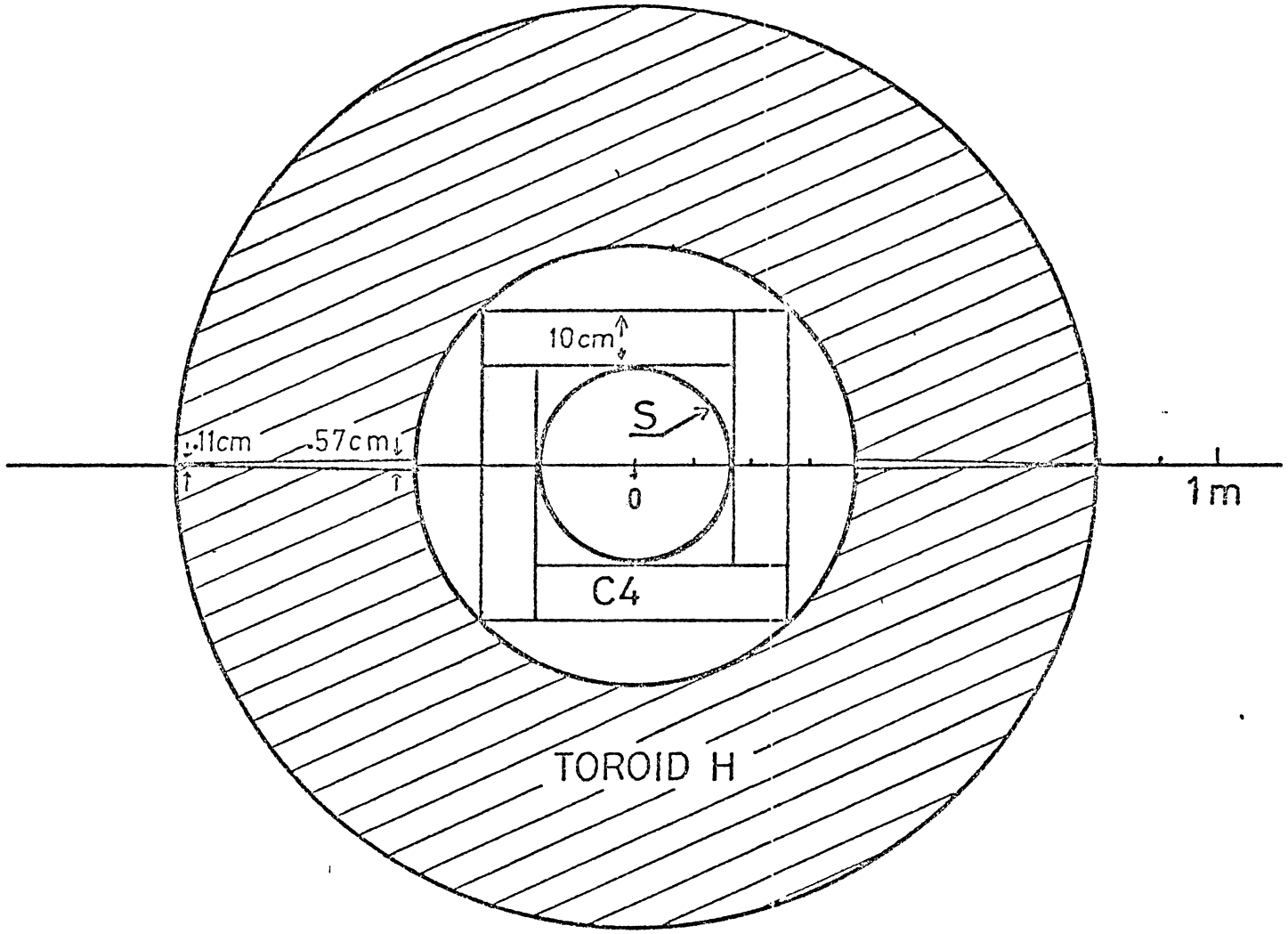

Fig. 3

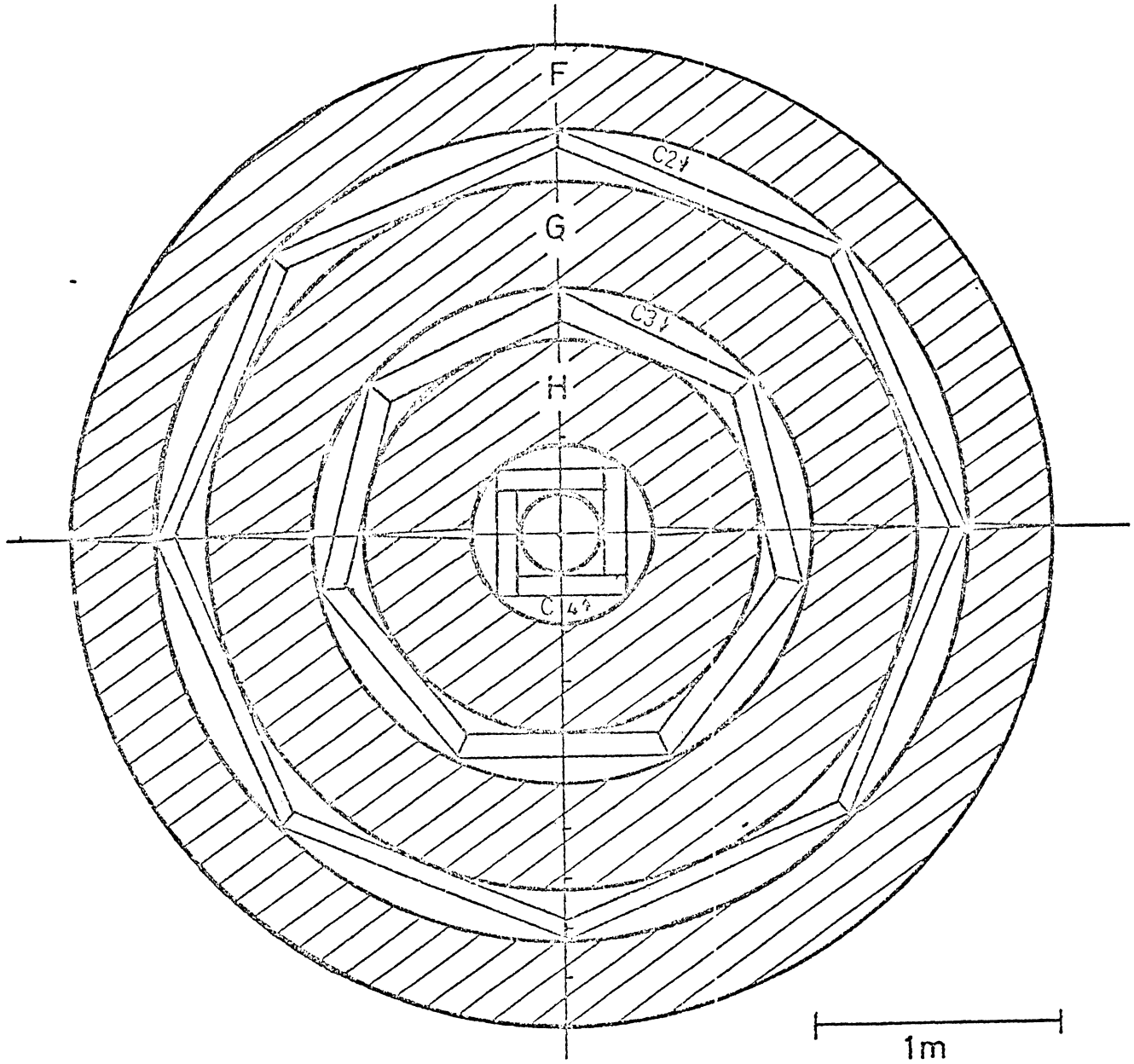

Fig. 4

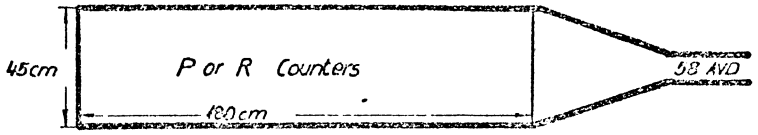

2cm thick

9 × 2 × 4 = 72 Counters

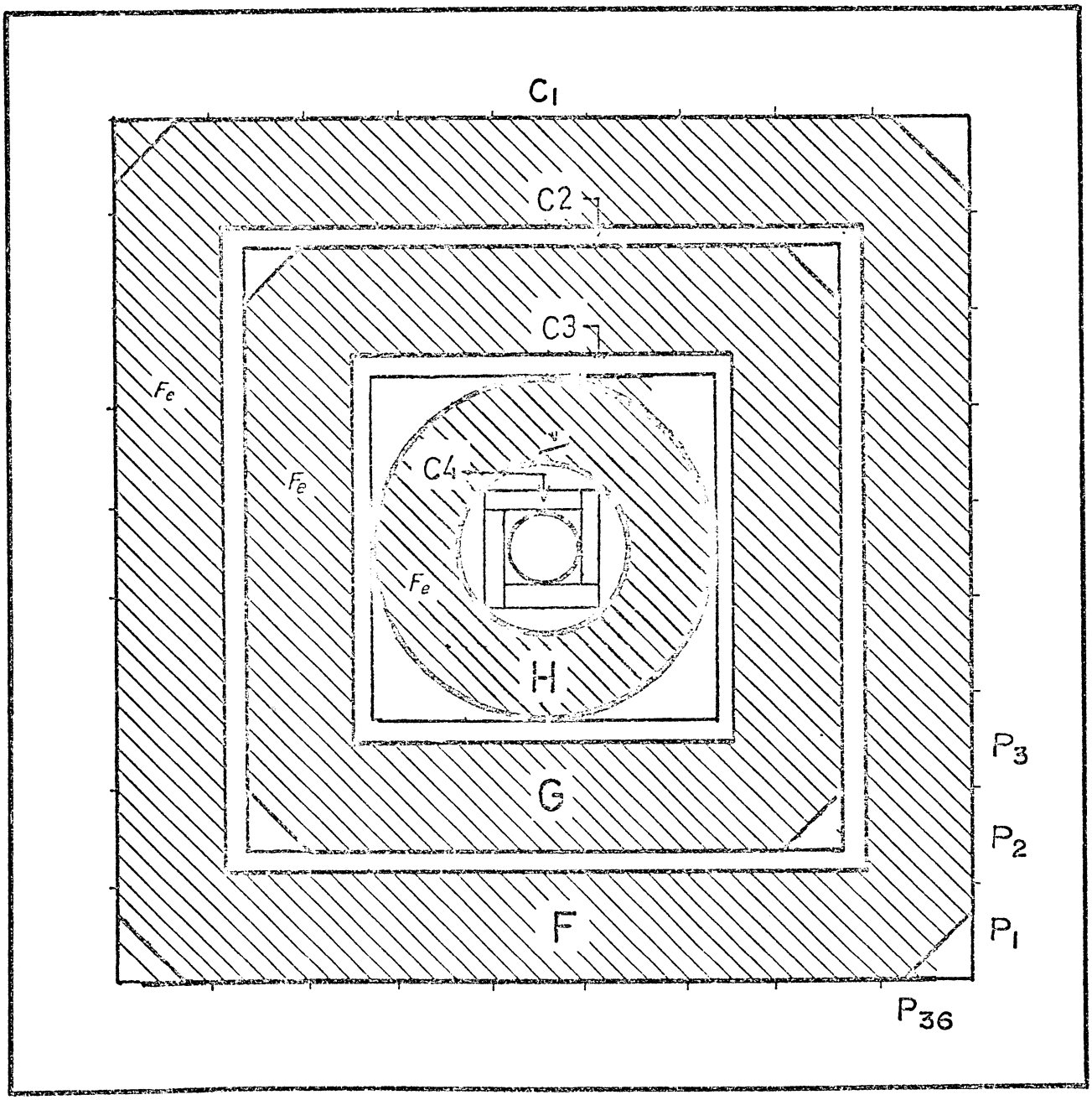

Fig 5

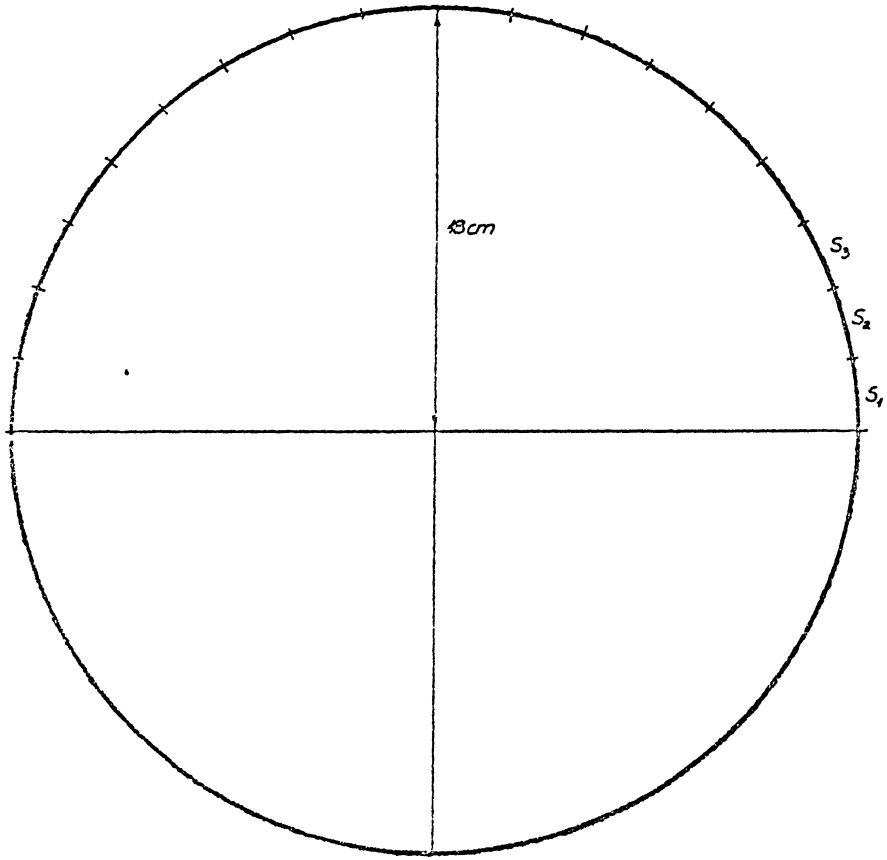

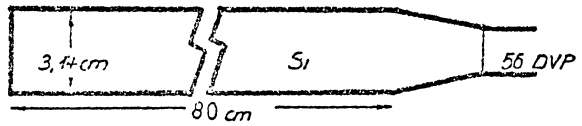

0,5 cm thick 36 Counter $\Delta\varphi = 10°$

Fig. 6a

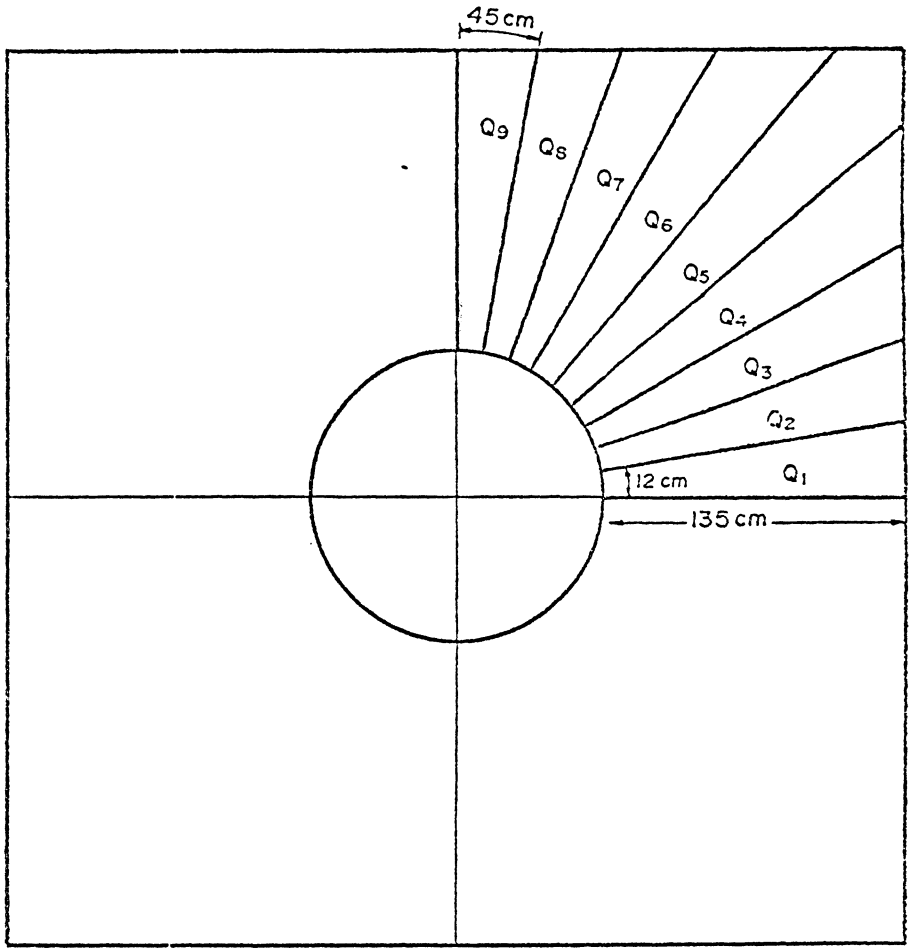

Fig. 6b

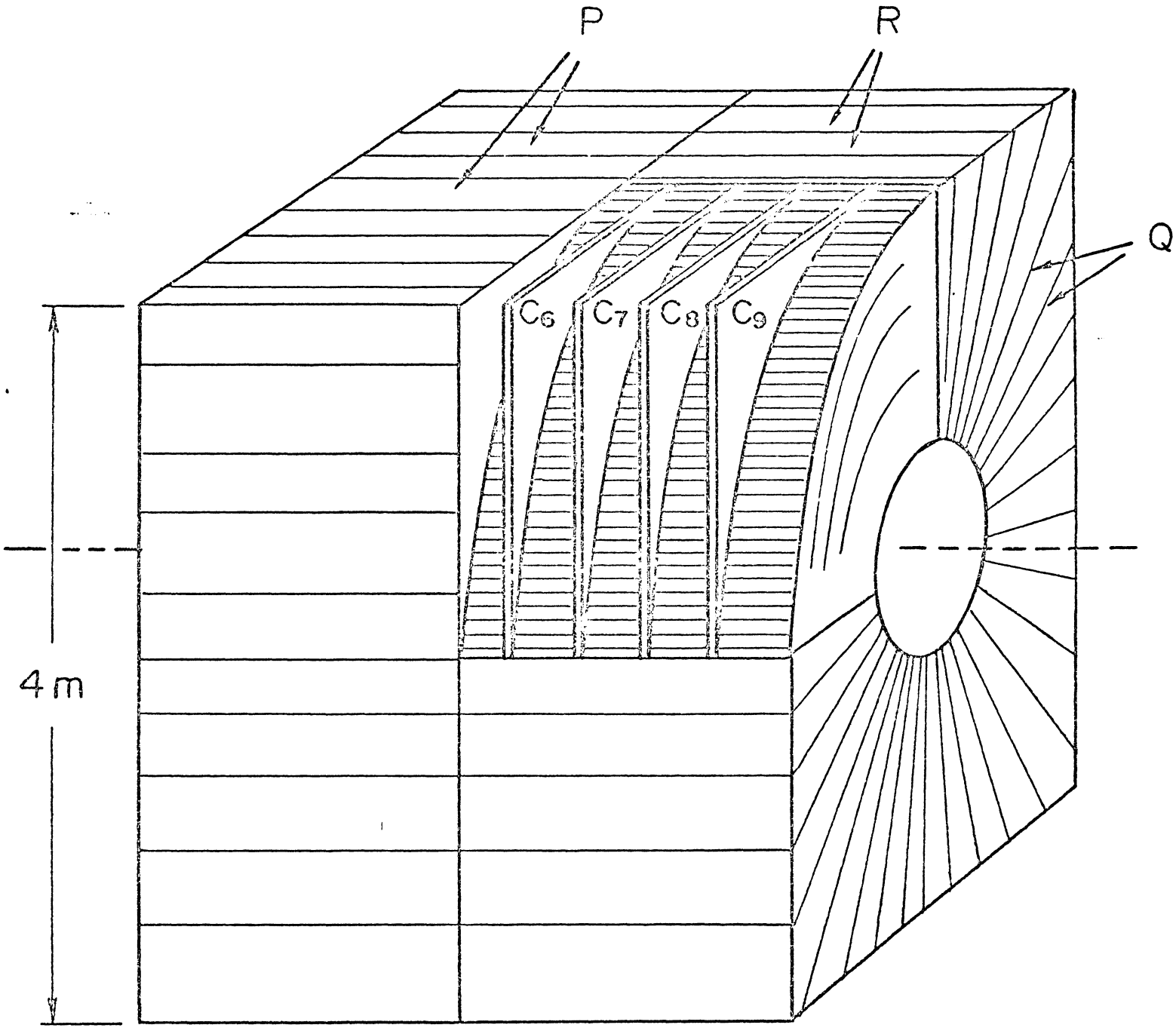

Fig. 7

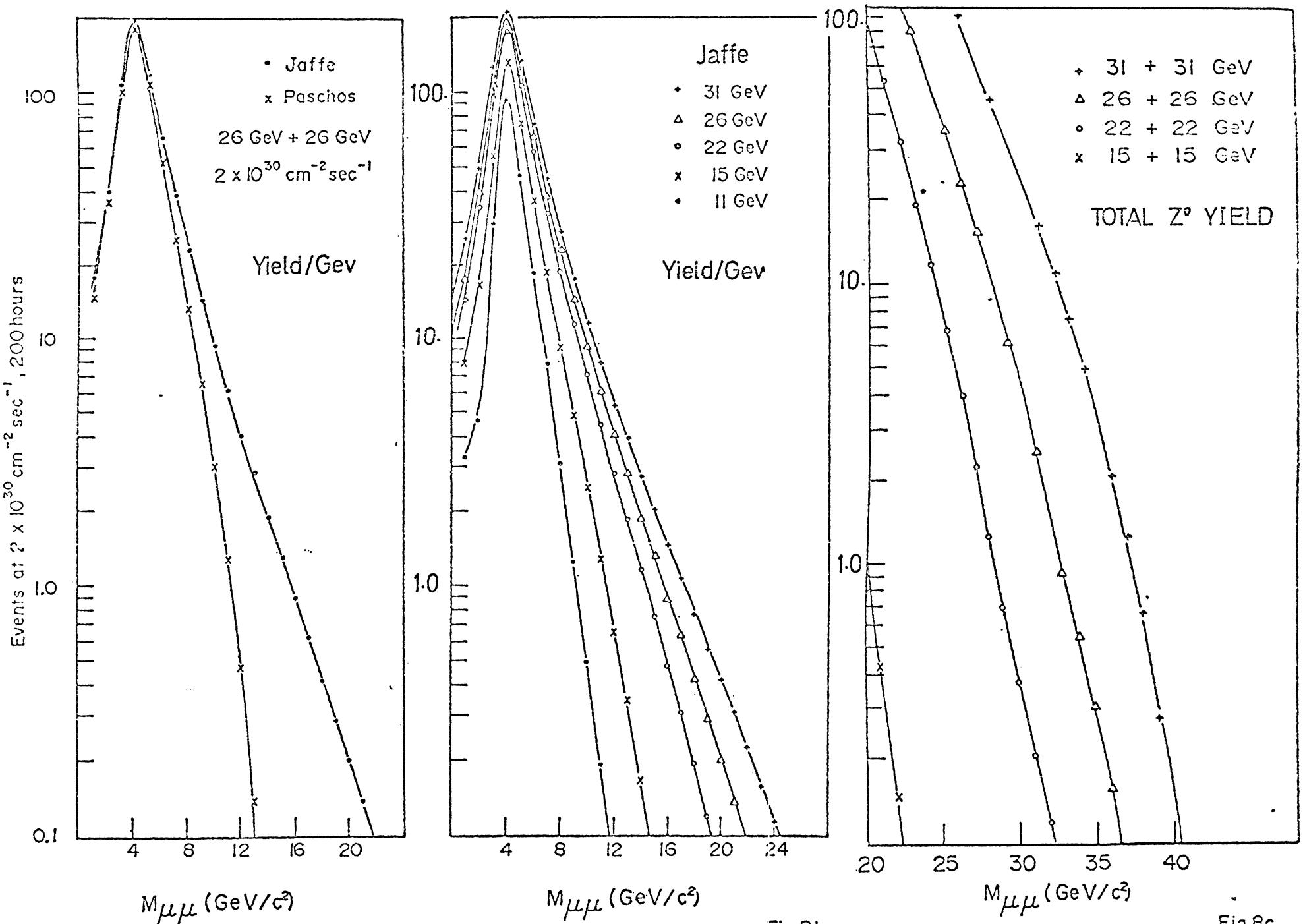

Fig 8a

Fig 8b

Fig 8c

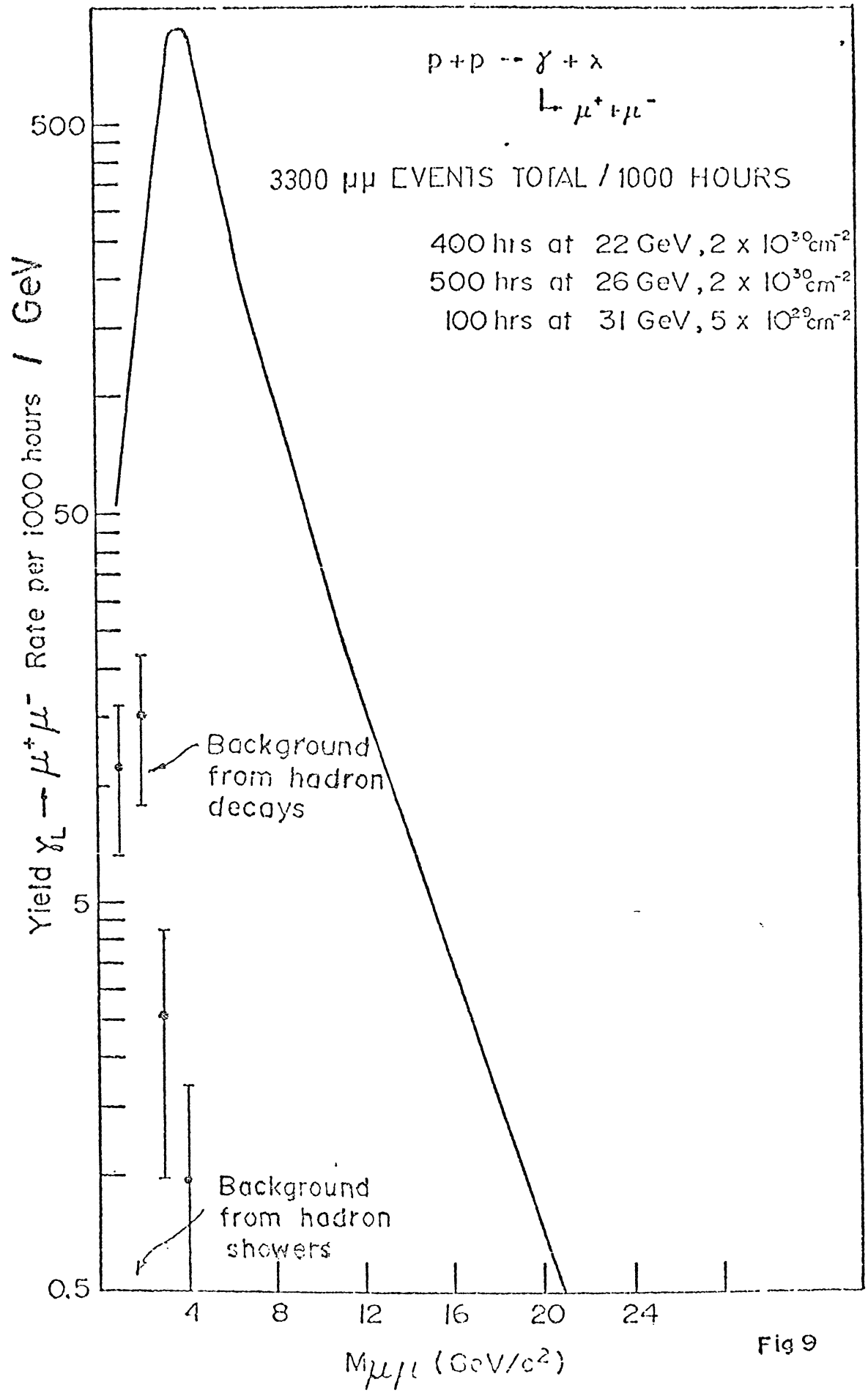
p + p → γ + λ
↳ μ⁺ + μ⁻
3300 μμ EVENTS TOTAL / 1000 HOURS
400 hrs at 22 GeV, 2 x 10³⁰ cm⁻²
500 hrs at 26 GeV, 2 x 10³⁰ cm⁻²
100 hrs at 31 GeV, 5 x 10²⁹ cm⁻²
Yield γL → μ⁺μ⁻ Rate per 1000 hours / GeV
500
50
5
0.5
Background from hadron decays
Background from hadron showers
4
8
12
16
20
24
Mμμ (GeV/c²)

Fig 9

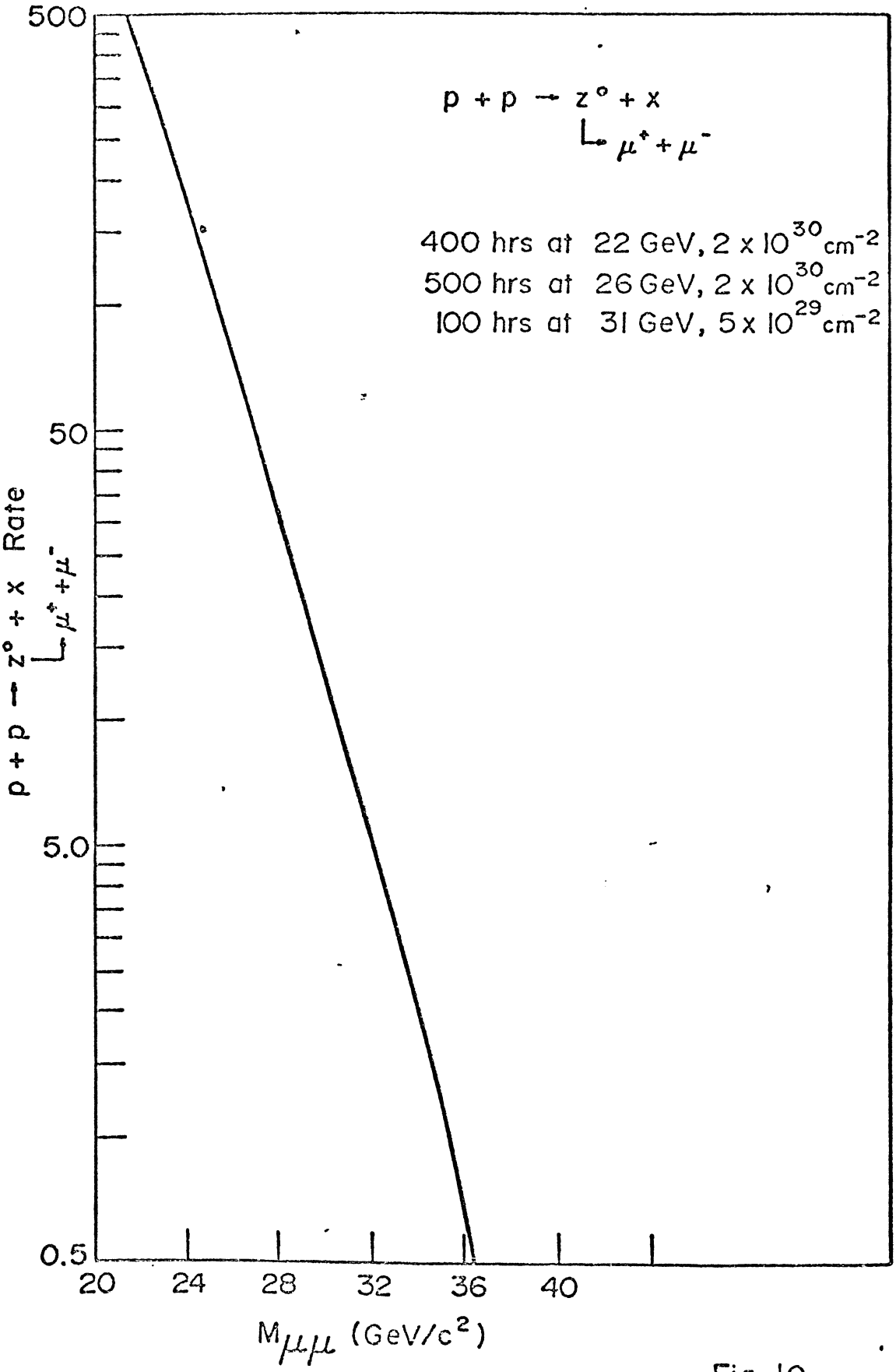
500
50
5.0
0.5
20
24
28
32
36
40
$p + p \rightarrow z^0 + x$
$\hookrightarrow \mu^+ + \mu^-$
400 hrs at 22 GeV, 2×10^{30} cm^{-2}
500 hrs at 26 GeV, 2×10^{30} cm^{-2}
100 hrs at 31 GeV, 5×10^{29} cm^{-2}
$p + p \rightarrow z^0 + x$ Rate
$\hookrightarrow \mu^+ + \mu^-$
$M_{\mu\mu}$ (GeV/c^2)

Fig. 10

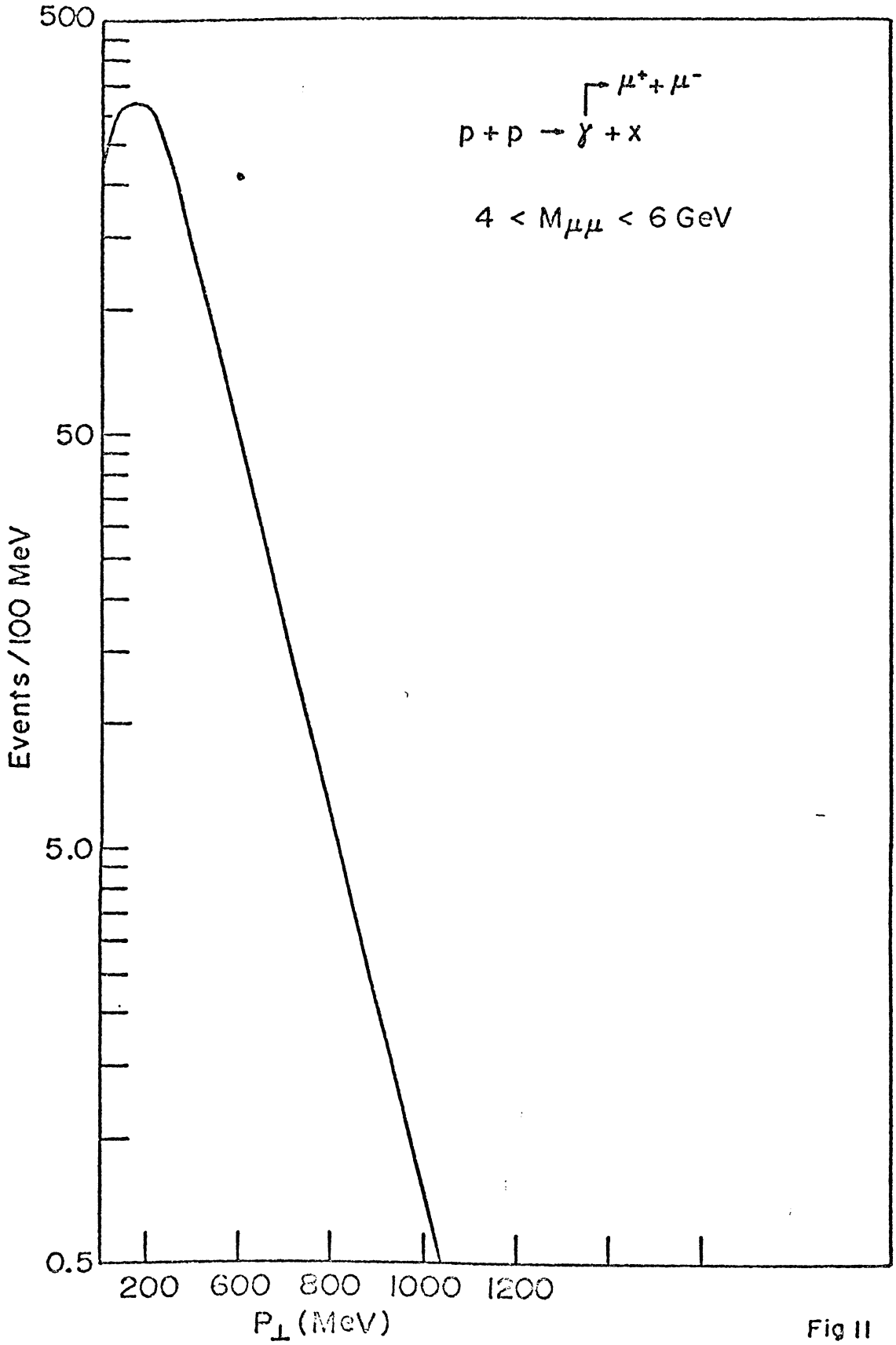
500
50
5.0
0.5
Events / 100 MeV
200
600
800
1000
1200
$P_\perp$ (MeV)
$p + p \rightarrow \gamma + x$
$\gamma \rightarrow \mu^+ + \mu^-$
$4 < M_{\mu\mu} < 6$ GeV

Fig 11

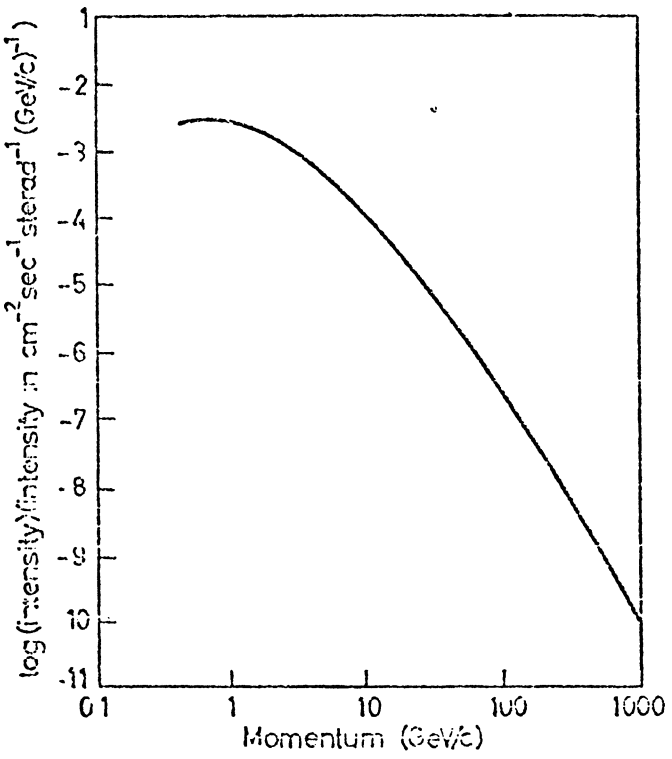
log (Intensity/Intensity in cm^{-2}sec^{-1}sterad^{-1}(GeV/c)$^{-1}$)
1
-2
-3
-4
-5
-6
-7
-8
-9
-10
-11
0.1
1
10
100
1000
Momentum (GeV/c)

Fig. 12

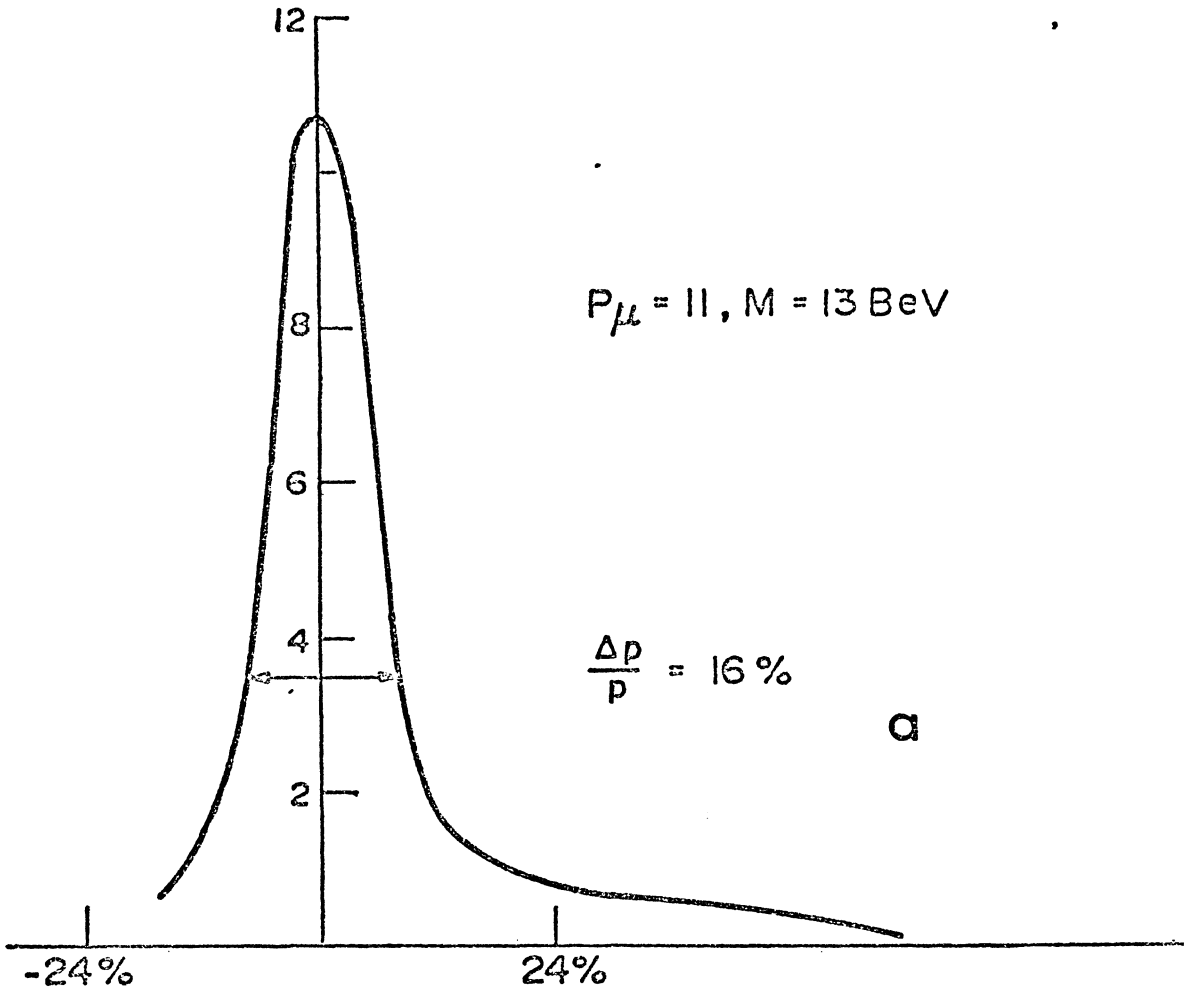
12
8
6
4
2
P_μ = 11, M = 13 BeV
$\frac{\Delta p}{p}$ = 16 %
a
-24%
24%

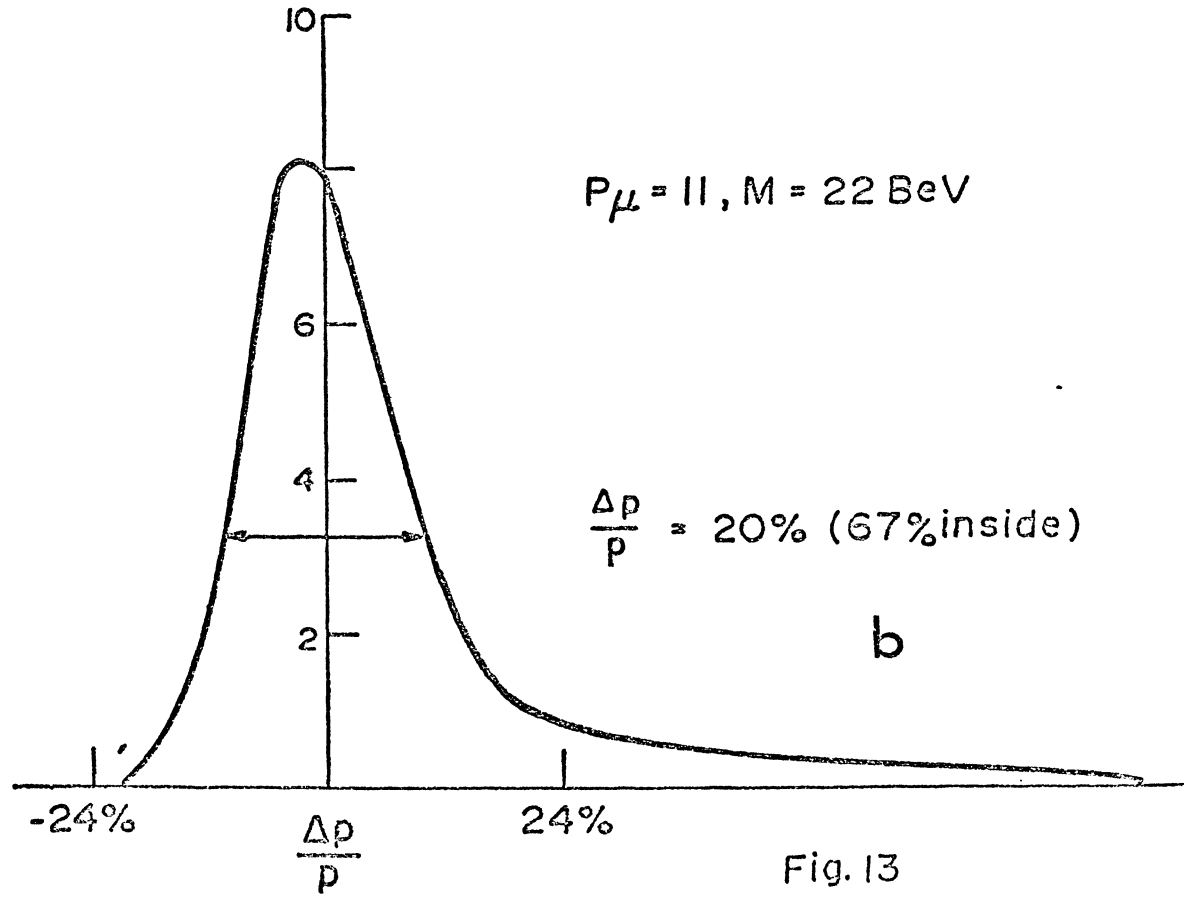
10
6
4
2
P_μ = 11, M = 22 BeV
$\frac{\Delta p}{p}$ = 20% (67% inside)
b
-24%
$\frac{\Delta p}{p}$
24%

Fig. 13